

Supporting Information

Understanding Electrochemical Reaction Mechanisms of Precious Metals Au and Ru as Cathode Catalyst in Li-CO₂ Batteries

Jian Hu^{a,b}, Chao Yang^a, Kunkun Guo^{a,*}

^a College of Materials Science and Engineering, Hunan University, Hunan joint international laboratory of advanced materials and technology for clean energy, Changsha 410082, People's Republic of China

^b Hunan Provincial Key Laboratory of Fine Ceramics and Powder Materials, School of Materials and Environmental Engineering, Hunan University of Humanities, Science and Technology, Loudi, Hunan 417000, People's Republic of China

*Corresponding author: Kunkunguo@hnu.edu.cn;

Table of Contents

S1. Adsorption energy	2
S2. Implicit Solvent	5
S3. Electronic structure analysis	6
S4. Standard Gibbs free energy and equilibrium potentials	6
S5. Gibbs free energy change during the nucleation processes of Li ₂ CO ₃ and Li ₂ C ₂ O ₄	6
S6. Gibbs free energy change during the decomposition process of Li ₂ CO ₃	16
S7. Electrochemical Free energy during the discharge and charge processes	17
References	18

S1. Adsorption energy

The optimized adsorption geometries of the intermediates are investigated for all reaction pathways. Here, as a typical example of the adsorption of Li atom, possible adsorption sites on the Au (111) and Ru (0001) surfaces are presented in Fig. S1, where A is the top sites of surface atoms (the first layer), B is the bridge sites between two surface neighbored atoms (the first layer), C and D are separately the hollow sites at the vertically top of the second and third layers, respectively, and E is the hollow sites located at the center positions among the three neighbored surface atoms together with the absence of atoms below the vertical.

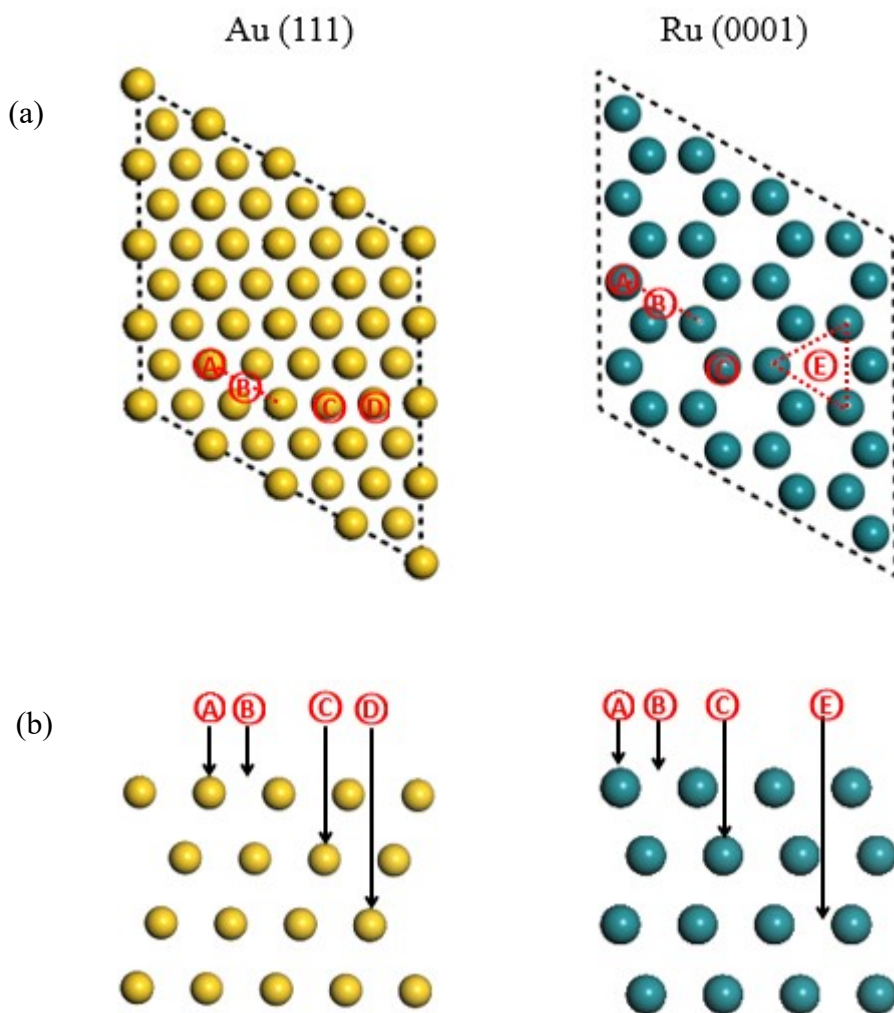


Fig. S1 Possible adsorption sites on the Au and Ru surfaces along the top (a) and side (b) views, Au (●) and Ru (●).

The calculated adsorption energies of Li and CO₂ molecules located at possible adsorptive sites on the surfaces of Au (111) and Ru (0001) are listed in Table S1, respectively. It is found that all the adsorption energies are

negative, indicating that these small molecules can be adsorptive on the Au and Ru surfaces, but CO₂ molecules are very weakly absorbed on both Au and Ru surfaces.

Table S1 Adsorption energies of Li and CO₂ molecules at different positions on Au (111) and Ru (0001) surfaces.

E_{ad} / eV	adsorbants	A	B	C	D	E
Au (111)	Li	-2.82	-3.08	-3.09	-3.10	/
	CO ₂	-0.235	-0.252	-0.254	-0.251	/
Ru (0001)	Li	-3.01	-3.14	-3.15	/	-3.14
	CO ₂	-0.36	-0.41	-0.52	/	-0.47

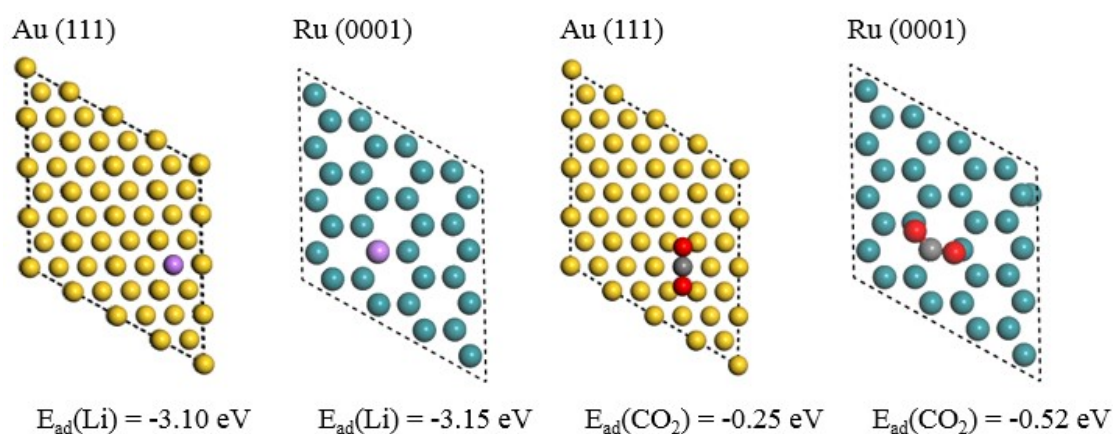


Fig. S2 The most stable adsorption configurations for Li and CO₂ adsorbed on Au (111) and Ru (0001) surfaces, Au (Au), Ru (Ru), C (C), O (O) and Li (Li).

Fig. S2 represents the most stable adsorption configurations for Li and CO₂ adsorbed on Au (111) and Ru (0001) surfaces. As shown in Table S1, in the case of Li atom, the adsorption energy $E_{ad}(\text{Li})$ for D site on Au (111) possess the lowest adsorptive energy of -3.10 eV, which is slightly lower than A site, but is approximate to both B and C sites. On the Ru (0001) surface, the adsorption energy $E_{ad}(\text{Li})$ of C site is the lowest energy of -3.15 eV, which is also slightly lower than A site, but is very close to both B and E sites. Therefore, our result shows that the most stable adsorption sites of Li adsorbed on the Au (111) and Ru (0001) surfaces are the hollow sites at the top of the third and second layers, respectively. Irrespective of Au and Ru surfaces, the adsorption energy of Li located at the top sites above the surface atoms possesses the weak adsorptive interactions between Li and metal surfaces, where for these configurations, the distances between the adsorbed Li atom and the Au or Ru surface atoms are measured to be 2.208 Å and 2.454 Å, respectively, which represent the longest distance among these adsorption sites due to the surface metal atoms below the adsorbed Li atom vertically.

In the case of CO₂ molecule, the adsorption energies of CO₂ molecular at the top sites (A) are also the weak adsorptive interactions for both Au (111) (-0.235 eV) and Ru (0001) (-0.36 eV) surfaces. The most stable

configurations of CO₂ adsorbed on these metal surfaces, C sites exhibit the lowest adsorptive energies for Au (111) (-0.254 eV) and Ru (0001) (-0.52 eV) surfaces, respectively. Therefore, the hollow sites at the vertical second layers for Au (111) and Ru (0001) are energetically more favorable for the adsorption of CO₂ molecules. In addition, during these favorable configurations, the distance between O atom and the neighbored Ru atom is measured about 2.09 Å, which is slightly shorter than the distance of C atom and Ru atom (2.26 Å). Likewise, the distance between O and the neighbored Au atom (3.38 Å) is also shorter than that between C and Au atom (3.66 Å). It is unexpectedly observed that the angle between C=O bonds on the Ru surface exhibits slightly twisted, but the angle on the Au surface still attains 180 degree. Further examination of the CO₂ adsorption on Ru surface shows that when we move the initial positions to adjust the distances between CO₂ and the Ru surface varying from 7.4 Å to 2 Å, the calculated adsorption energy is close to zero at the distance of 7.4 Å, and then becomes -0.52 eV at the distance less than 7.4 Å together with the appearance of the twisted angles between C=O bonds. The phenomena is also observed experimentally that the adsorption of CO₂ and Ru surface is confirmed to the change of the bond angle, but the bond angle between C=O bonds cannot be changed at the adsorption between CO₂ and Au.^{1,2} Likewise, the C=O bond length of CO₂ molecules is found to elongate from 1.162 Å to 1.301 Å absorbed on Ru (0001) and maintain the length about 1.177 Å on Au (111), respectively.

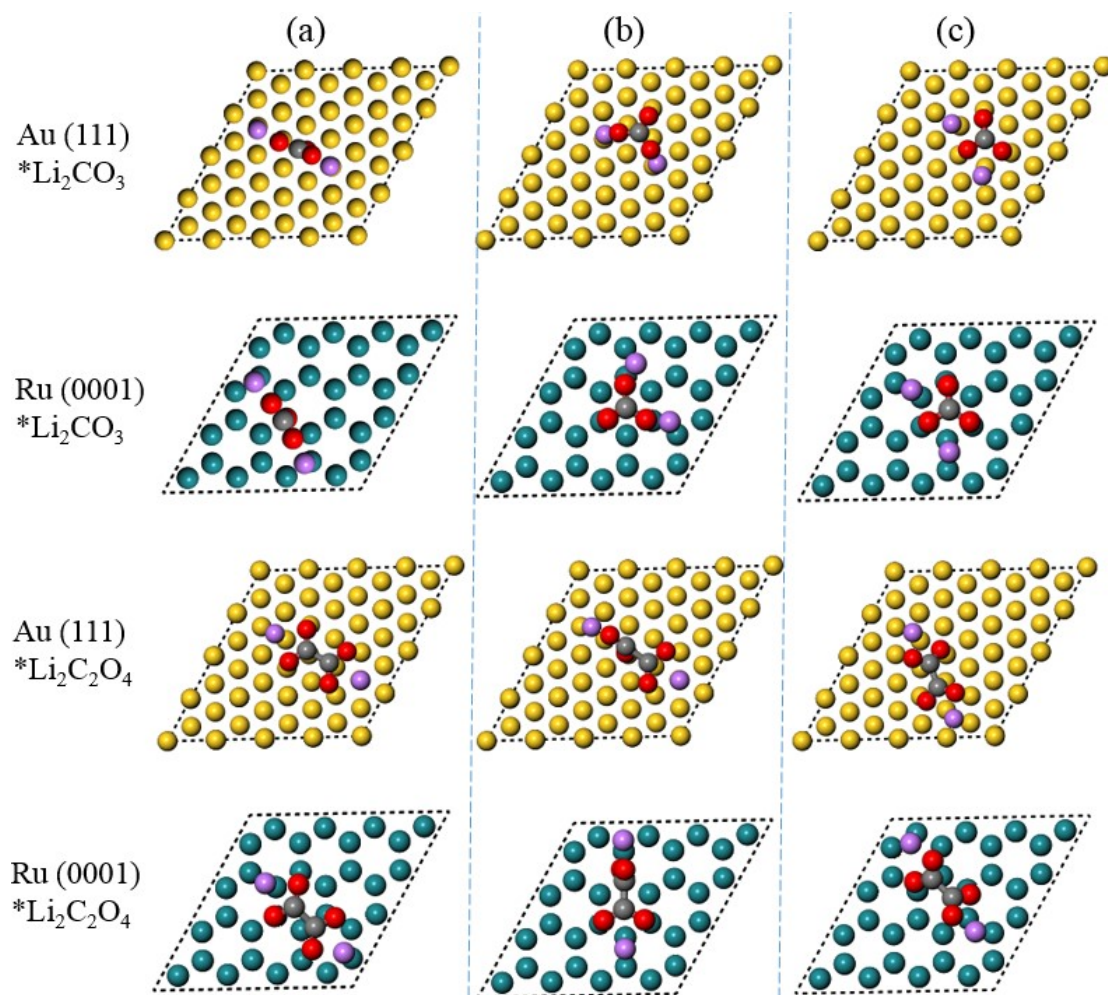


Fig. S3 Possible adsorption sites for Li_2CO_3 and $\text{Li}_2\text{C}_2\text{O}_4$ on Au (111) and Ru (0001) surfaces, Au (Au), Ru (Ru), C (C), O (O) and Li (Li).

Possible adsorption sites are constructed on two metallic surfaces. A lot of adsorption sites are tried, but Li_2CO_3 and $\text{Li}_2\text{C}_2\text{O}_4$ molecules would tend to fall apart. Therefore, typical initial configurations are chosen as shown in Fig. S3. Compared with the adsorption energies, the most stable configurations are obtained as shown in Fig. S4. For the adsorption of Li_2CO_3 on Au and Ru surfaces, the three O atoms of CO_3^{2-} are located directly above the metallic atoms, and the Li atoms are located above the vacancy sites. The distances between O atoms and the surface atoms on Au (111) and Ru (0001) surfaces are 2.41 Å and 2.22 Å, respectively. In the adsorption of $\text{Li}_2\text{C}_2\text{O}_4$, $\text{C}_2\text{O}_4^{2-}$ behaves like two bended CO_2 molecules bound by a certain angle, where two O atoms are close to the metallic surfaces and directly above the surface metal atoms, while the remaining two O atoms are far away from the metallic surfaces. The distance between the two O atoms near the surface and the Au (111) and Ru (0001) surface atoms is 2.54 Å and 2.18 Å, respectively. In addition, the adsorption energies of Li_2CO_3 and $\text{Li}_2\text{C}_2\text{O}_4$ on Au (111) surface are -1.98 eV and -1.72 eV, respectively, which are larger than those of -3.37 eV and -3.08 eV on Ru (0001) surface.

Table S2 Adsorption energies of Li_2CO_3 and $\text{Li}_2\text{C}_2\text{O}_4$ molecules at different positions on Au (111) and Ru (0001) surfaces.

$E_{\text{ad}} / \text{eV}$	adsorbants	a	b	c
Au (111)	Li_2CO_3	-1.19	-1.53	-1.98
	$\text{Li}_2\text{C}_2\text{O}_4$	-1.63	-1.28	-1.72
Ru (0001)	Li_2CO_3	-2.63	-2.86	-3.37
	$\text{Li}_2\text{C}_2\text{O}_4$	-3.03	-2.52	-3.08

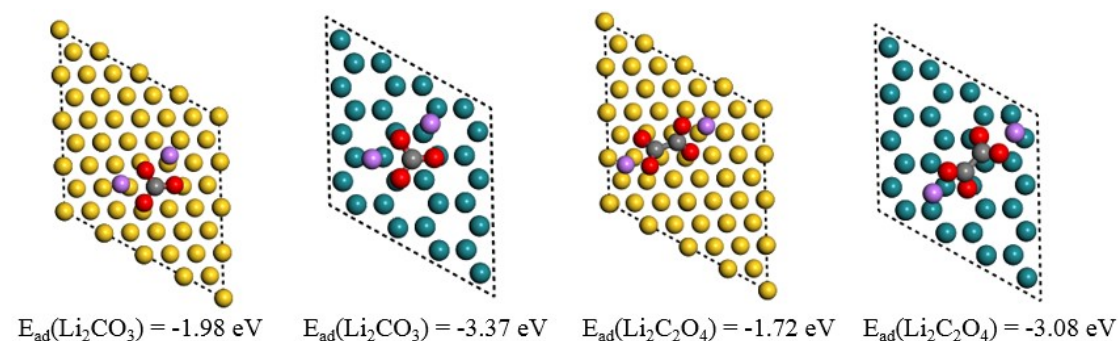


Fig. S4 The most stable adsorption configurations for Li_2CO_3 and $\text{Li}_2\text{C}_2\text{O}_4$ adsorbed on Au (111) and Ru (0001) surfaces, Au (Au), Ru (Ru), C (C), O (O) and Li (Li).

S2. Implicit Solvent

Dimethyl sulfoxide (DMSO, the relative dielectric constant $\epsilon = 49$) is reported as the electrolyte solvent with Au and Ru precious metal as cathode catalysts in Li- CO_2 battery.³ In order to study the effect of solvents, DMSO solvent is implicitly modeled by a polarizable dielectric continuum as implemented in the VASPsol code. Meanwhile, the adsorption energies of Li, CO_2 , Li_2CO_3 and $\text{Li}_2\text{C}_2\text{O}_4$ on two Au (111) and Ru (0001) surfaces are calculated in implicit solvent and vacuum environments as listed in Table S3. As shown in Table S3, compared with the vacuum environments, the adsorption energies of Li on the two surfaces is found to increase about 0.7 eV in implicit solvents, while the adsorption energies of CO_2 , Li_2CO_3 and $\text{Li}_2\text{C}_2\text{O}_4$ increase less than 0.1 eV on both Au (111) and Ru (0001) surfaces.

Table S3 Adsorption energy of Li, CO_2 , Li_2CO_3 and $\text{Li}_2\text{C}_2\text{O}_4$ in vacuum and solvent environment on Au (111) and Ru (0001) surfaces, respectively.

catalytic surface		environment	Li	CO_2	Li_2CO_3	$\text{Li}_2\text{C}_2\text{O}_4$
Au (111)	η_0/eV	vacuum	-3.10	-0.25	-1.98	-1.72
		DMSO	-3.81	-0.27	-2.06	-1.79
Ru (0001)	η_0/eV	vacuum	-3.15	-0.52	-3.37	-3.08
		DMSO	-3.84	-0.57	-3.46	-3.14

S3. Electronic structure analysis

Project density of states (DOS) analysis is used to describe the electronic structures changes for Li, CO₂, Li₂CO₃ and Li₂C₂O₄ molecules before and after the adsorptions on two metallic surfaces. Fig. S5 shows the projected density of states of these isolated molecules and the Au (111) and Ru (0001) substrate.

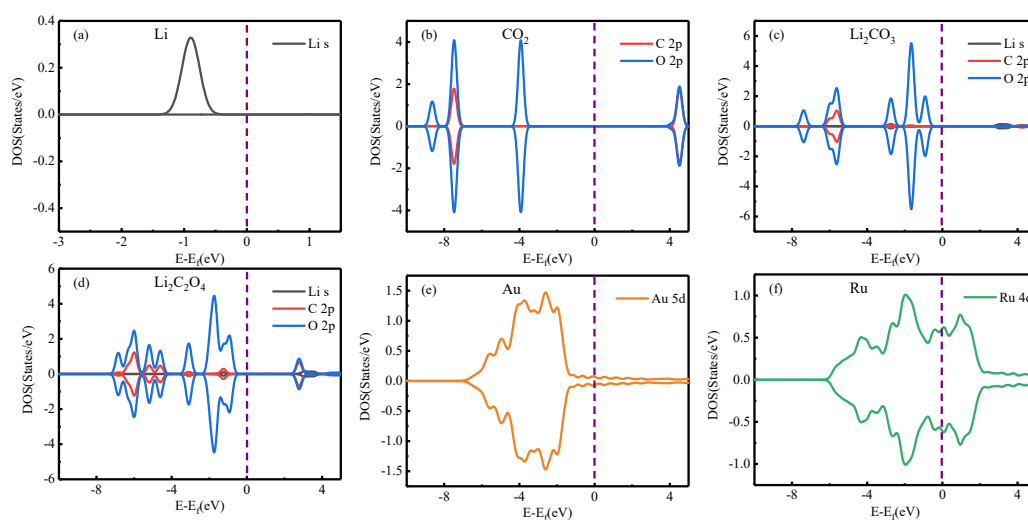
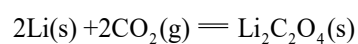


Fig. S5 Density of states for the isolated Li, CO₂, Li₂CO₃ and Li₂C₂O₄ molecules and the Au (111) and Ru (0001) substrates.

S4. Standard Gibbs free energy and equilibrium potentials

As reported in our previous studies⁴, the standard Gibbs free energy (ΔG_f^0) for



and



are - 5.74 eV for Li₂CO₃ and -6.02 eV for Li₂C₂O₄, respectively. According to the Nernst equation of $U_0(\text{M}) = -\Delta G_f^0(\text{M}) / ne$, the equilibrium potentials, $U_0(\text{Li}_2\text{CO}_3)$ and $U_0(\text{Li}_2\text{C}_2\text{O}_4)$, are calculated to be separately 2.87 V for Li₂CO₃ and 3.01 V for Li₂C₂O₄.

S5. Gibbs free energy change during the nucleation processes of Li_2CO_3 and $\text{Li}_2\text{C}_2\text{O}_4$

The nucleation processes of Li_2CO_3 and $\text{Li}_2\text{C}_2\text{O}_4$ on different catalytic surfaces are estimated by the Gibbs free energy change (ΔG_f) between different intermediates on different catalytic surfaces. Possible reaction pathways presented in Table S4 are designed according the previous publication, where three cases are divided that pathways I are interpreted as the first adsorption of Li atom and second adsorption of CO_2 molecule, pathways II are interpreted as the first adsorption of CO_2 molecule and second adsorption of Li atom, pathways III are interpreted as the preferred adsorptions of CO_2 during the first two intermediary steps.³⁻⁷

Table S4 Possible reaction pathways.

Reaction pathway		Path name	Reaction pathway		Path name
$*\text{Li} \xrightarrow{+\text{CO}_2} *\text{LiCO}_2$	$\xrightarrow{+\text{Li}} *\text{Li}_2\text{CO}_2 \xrightarrow{+\text{CO}_2} *\text{Li}_2\text{CO}_3 + *\text{CO}$	I	$*\text{CO}_2 \xrightarrow{+\text{Li}} *\text{LiCO}_2$	$\xrightarrow{+\text{CO}_2} *\text{LiCO}_3 \xrightarrow{+\text{Li}} *\text{Li}_2\text{CO}_3 + *\text{CO}$	II
	$\xrightarrow{+\text{Li}} *\text{Li}_2\text{CO}_2 \xrightarrow{+\text{CO}_2} *\text{Li}_2\text{C}_2\text{O}_4$	I'		$\xrightarrow{+\text{Li}} *\text{Li}_2\text{CO}_2 \xrightarrow{+\text{CO}_2} *\text{Li}_2\text{C}_2\text{O}_4$	II'
	$\xrightarrow{+\text{CO}_2} *\text{LiCO}_3 \xrightarrow{+\text{Li}} *\text{Li}_2\text{CO}_3 + *\text{CO}$	I''		$\xrightarrow{+\text{Li}} *\text{Li}_2\text{CO}_2 \xrightarrow{+\text{CO}_2} *\text{Li}_2\text{CO}_3 + *\text{CO}$	II''
	$\xrightarrow{+\text{CO}_2} *\text{LiC}_2\text{O}_4 \xrightarrow{+\text{Li}} *\text{Li}_2\text{C}_2\text{O}_4$	I'''		$\xrightarrow{+\text{CO}_2} *\text{LiC}_2\text{O}_4 \xrightarrow{+\text{Li}} *\text{Li}_2\text{C}_2\text{O}_4$	II'''
$*\text{CO}_2 \xrightarrow{+\text{CO}_2} *\text{CO}_3 \xrightarrow{+\text{Li}} *\text{LiCO}_3 \xrightarrow{+\text{Li}} *\text{Li}_2\text{CO}_3 + *\text{CO}$	III		$*\text{CO}_2 \xrightarrow{+\text{CO}_2} *\text{C}_2\text{O}_4 \xrightarrow{+\text{Li}} *\text{LiC}_2\text{O}_4 \xrightarrow{+\text{Li}} *\text{Li}_2\text{C}_2\text{O}_4$	III'	

*M indicates adsorbate on the catalyst surface.

In particular, CO as the intermediate is formed on different catalytic surfaces along with the nucleation process of Li_2CO_3 . Subsequently, the disproportionation reaction of CO produces C and CO_2 as listed in Eq. (2). The Gibbs free energies of CO disproportionation reaction on Au (111) and Ru (0001) surfaces are calculated as 0.06 and 0.24 eV, respectively, but the energy barriers are also calculated as 0.17 and 0.69 eV for Au (111) and Ru (0001) surfaces by CINEB method.



The Gibbs free energy changes for different intermediary steps are calculated on the basis of the following equation(3):

$$\Delta G_f(n) = \Delta E_{\text{tol}}(n) + \Delta E_{\text{zpc}}(n) - T\Delta S(n) - eU \quad (3)$$

where n represents the corresponding reaction step ($n = 1, 2, 3, 4, \dots$), while $\Delta E_{\text{tol}}(n)$, $\Delta E_{\text{zpc}}(n)$ and $\Delta S(n)$ are the DFT total energy difference, zero point correction energy difference, and entropy change under standard conditions ($T = 298 \text{ K}$) in different intermediary step n, respectively. A pre- and post-processing

program for VASP (VASPKIT), is employed to analyze zero point correction energy and entropy.⁸ As reported previously,⁴ zero point correction energy difference $\Delta E_{zpe}(n)$, entropy change $\Delta S(n)$ and the DFT total energy difference $\Delta E_{tol}(n)$ for every intermediary steps can be obtained from the minus between the product and reactants.⁹ The entropy of CO₂ and O₂ molecules under standard condition (T=298 K) is 213.8 J K⁻¹ mol⁻¹ and 205.1 J·K⁻¹ mol⁻¹ taken from the NIST database, and then the calculated entropy change of CO₂ and O₂ (TΔS) at 298 K is 0.66 eV and 0.63 eV, respectively. The potential of a solvation Li⁺ and an electron e in the electrode is set to be 0, which is balanced with the bulk Li. Therefore, the free energy of an electron together with the adsorption of Li⁺ depends on the applied potential of U and then will be shifted by $-eU$.⁸ The DFT total energy difference $\Delta E_{tol}(n)$, zero point correction energy difference $\Delta E_{zpe}(n)$, and entropy change under standard conditions (TΔS(n)) for every intermediary steps on two catalytic surfaces are presented in Table S5 – S6 and the corresponding Gibbs free energy changes calculated are shown in Fig. S6 – S11.

Table S5 Detailed reaction steps and the corresponding ΔE_{tol} (eV), ΔE_{zpe} (eV), TΔS (eV) during the nucleation processes of Li₂CO₃ or Li₂C₂O₄ on Au (111) surface

	Reaction step	ΔE_{tol} (eV)	ΔE_{zpe} (eV)	TΔS (eV)
I	Au + Li ⁺ + e ⁻ → *Li	-3.10	0.041	0.08
	*Li + CO ₂ → *LiCO ₂	-0.56	0.019	-0.43
	*LiCO ₂ + Li ⁺ + e ⁻ → *Li ₂ CO ₂	-3.46	0.043	0.05
	*Li ₂ CO ₂ + CO ₂ → *Li ₂ CO ₃ + *CO	0.04	0.002	-0.44
I'	Au + Li ⁺ + e ⁻ → *Li	-3.10	0.041	0.08
	*Li + CO ₂ → *LiCO ₂	-0.56	0.019	-0.43
	*LiCO ₂ + Li ⁺ + e ⁻ → *Li ₂ CO ₂	-2.94	0.034	0.12
	*Li ₂ CO ₂ + CO ₂ → *Li ₂ C ₂ O ₄	-0.43	0.049	-0.59
I''	Au + Li + e → *Li	-3.10	0.041	0.08
	*Li + CO ₂ → *LiCO ₂	-0.56	0.019	-0.43
	*LiCO ₂ + CO ₂ → *LiCO ₃ + *CO	0.83	0.027	-0.49
	*LiCO ₃ + *CO + Li ⁺ + e ⁻ → *Li ₂ CO ₃ + *CO	-4.24	0.018	0.10
I'''	Au + Li ⁺ + e ⁻ → *Li	-3.10	0.041	0.08
	*Li + CO ₂ → *LiCO ₂	-0.56	0.019	-0.43
	*LiCO ₂ + CO ₂ → *LiC ₂ O ₄	0.11	0.012	-0.33
	*LiC ₂ O ₄ + Li ⁺ + e ⁻ → *Li ₂ C ₂ O ₄	-3.48	0.070	-0.14
II	Au + CO ₂ → *CO ₂	-0.25	0.008	-0.40
	*CO ₂ + Li ⁺ + e ⁻ → *LiCO ₂	-3.40	0.051	0.05
	*LiCO ₂ + CO ₂ → *LiCO ₃ + *CO	0.83	0.027	-0.49
	*LiCO ₃ + *CO + Li ⁺ + e ⁻ → *Li ₂ CO ₃ + *CO	-4.24	0.018	0.10
II'	Au + CO ₂ → *CO ₂	-0.25	0.008	-0.40
	*CO ₂ + Li ⁺ + e ⁻ → *LiCO ₂	-3.40	0.051	0.05
	*LiCO ₂ + Li ⁺ + e ⁻ → *Li ₂ CO ₂	-2.94	0.034	0.12

	$*\text{Li}_2\text{CO}_2 + \text{CO}_2 \rightarrow *\text{Li}_2\text{C}_2\text{O}_4$	-0.43	0.049	-0.59
	$\text{Au} + \text{CO}_2 \rightarrow *\text{CO}_2$	-0.25	0.008	-0.40
II''	$*\text{CO}_2 + \text{Li}^+ + \text{e}^- \rightarrow *\text{LiCO}_2$	-3.40	0.051	0.05
	$*\text{LiCO}_2 + \text{Li}^+ + \text{e}^- \rightarrow *\text{Li}_2\text{CO}_2$	-3.46	0.043	0.05
	$*\text{Li}_2\text{CO}_2 + \text{CO}_2 \rightarrow *\text{Li}_2\text{CO}_3 + *\text{CO}$	0.04	0.002	-0.44
	$\text{Au} + \text{CO}_2 \rightarrow *\text{CO}_2$	-0.25	0.008	-0.40
II'''	$*\text{CO}_2 + \text{Li}^+ + \text{e}^- \rightarrow *\text{LiCO}_2$	-3.40	0.051	0.05
	$*\text{LiCO}_2 + \text{CO}_2 \rightarrow *\text{Li}_2\text{C}_2\text{O}_4$	0.11	0.012	-0.33
	$*\text{Li}_2\text{C}_2\text{O}_4 + \text{Li}^+ + \text{e}^- \rightarrow *\text{Li}_2\text{C}_2\text{O}_4$	-3.48	0.070	-0.14
III	$\text{Au} + \text{CO}_2 \rightarrow *\text{CO}_2$	-0.25	0.008	-0.40
	$*\text{CO}_2 + \text{CO}_2 \rightarrow *\text{CO}_3 + *\text{CO}$	0.37	0.009	-0.41
	$*\text{CO}_3 + *\text{CO} + \text{Li}^+ + \text{e}^- \rightarrow *\text{LiCO}_3 + *\text{CO}$	-2.94	0.069	-0.03
	$*\text{LiCO}_3 + *\text{CO} + \text{Li}^+ + \text{e}^- \rightarrow *\text{Li}_2\text{CO}_3 + *\text{CO}$	-4.24	0.018	0.10
III'	$\text{Au} + \text{CO}_2 \rightarrow *\text{CO}_2$	-0.25	0.008	-0.40
	$*\text{CO}_2 + \text{CO}_2 \rightarrow *\text{C}_2\text{O}_4$	0.01	0.007	-0.40
	$*\text{C}_2\text{O}_4 + \text{Li}^+ + \text{e}^- \rightarrow *\text{Li}_2\text{C}_2\text{O}_4$	-3.30	0.056	0.12
	$*\text{Li}_2\text{C}_2\text{O}_4 + \text{Li}^+ + \text{e}^- \rightarrow *\text{Li}_2\text{C}_2\text{O}_4$	-3.48	0.070	-0.14

*M indicates adsorbate on the catalytic surface.

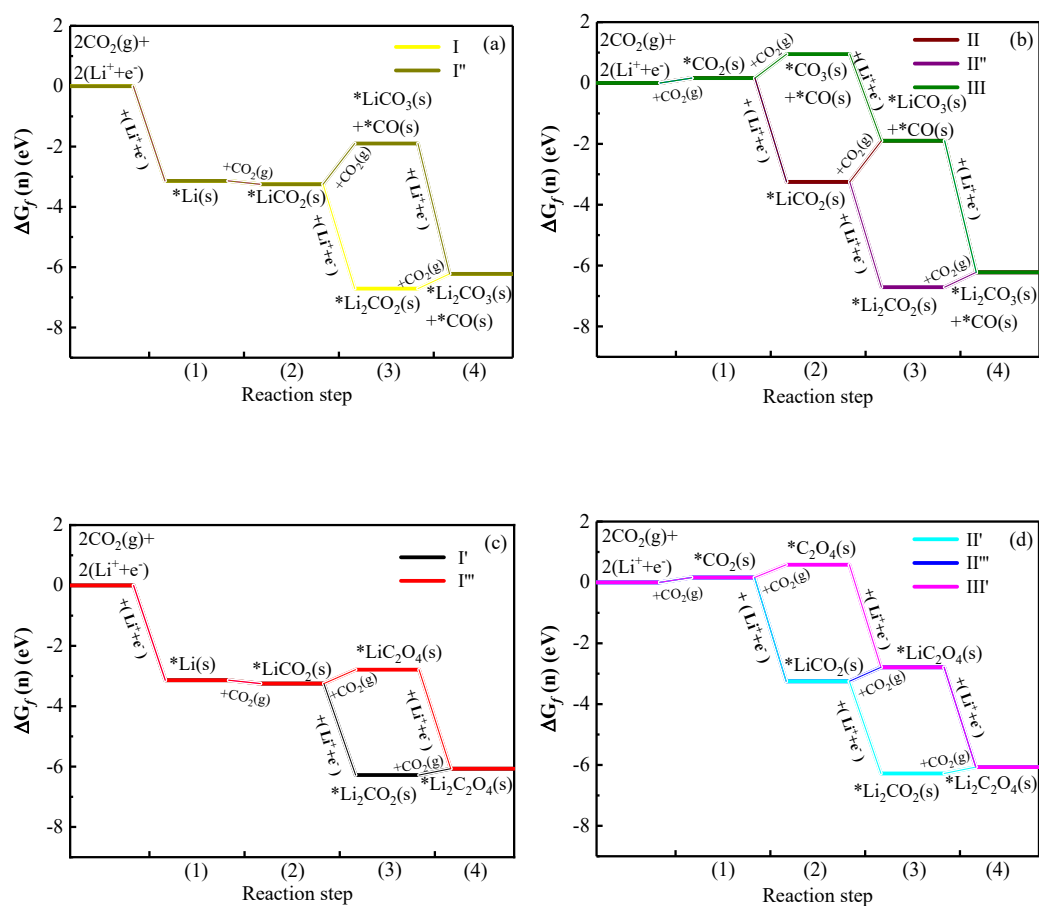


Fig. S6 Calculated energetic profiles ($\Delta G_f(n)$) for the nucleations of Li_2CO_3 ((a) - (b)) and $\text{Li}_2\text{C}_2\text{O}_4$ ((c) - (d)) on

the Au (111) surface at an open circuit potential ($U = 0$ V). *M denotes adsorbate on the catalytic surface.

Fig. S6 shows the calculated Gibbs free energetic profiles ($\Delta G_f(n)$) for the nucleation processes of both Li_2CO_3 and $\text{Li}_2\text{C}_2\text{O}_4$ on the Au (111) surface at $U = 0$ V. It is found that in all pathways, the steps related with Li atoms are all downhill in the energy profiles. Inspection of all pathways whose intermediary steps are related with CO_2 molecule shows that if the first step is CO_2 adsorption, the free energy increases about 0.16 eV, as well as the intermediary steps containing the formation of carbonate (CO_3^{2-}) and oxalate ($\text{C}_2\text{O}_4^{2-}$) are always endothermic, while other steps are still downhill in the energy profiles. Additionally, the maximum increased energies for every intermediary steps during all pathways of Li_2CO_3 nucleations are the intermediary steps to form a carbonate which are 0.49, 1.35, 0.49, 1.35 and 0.79 eV for the pathways I, I', II', II and III, respectively, and those maximum increased energies during all pathways of $\text{Li}_2\text{C}_2\text{O}_4$ nucleations are the steps to form an oxalate, which are 0.21, 0.46, 0.46, 0.21 and 0.42 eV for the pathways I', I'', II'', II' and III', respectively. Therefore, we can conclude that during the nucleation processes of both Li_2CO_3 and $\text{Li}_2\text{C}_2\text{O}_4$ (Fig. S6 (a) - (d)), the steps involving the formation of CO_3^{2-} and $\text{C}_2\text{O}_4^{2-}$ are the kinetically controlling steps at $U = 0$ V, respectively. Meanwhile, the energy barriers during the steps to form oxalate are all found to be significantly less than those to form carbonate.

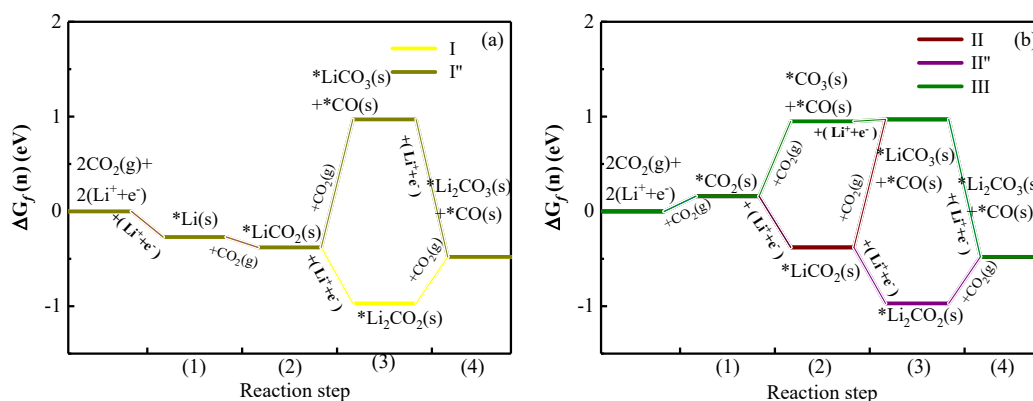


Fig. S7 Calculated energetic profiles of Li_2CO_3 nucleations on the Au (111) surface at $U = U_0(\text{Li}_2\text{CO}_3) = 2.87$ V.

The Gibbs free energetic profiles of Li_2CO_3 nucleations on the Au (111) surface are shown in Fig. S7 under the equilibrium potential ($U_0(\text{Li}_2\text{CO}_3) = 2.87$ V). The first adsorption of CO_2 molecule on the Au (111) surface as the first step during Li_2CO_3 nucleations still remain endothermic with the increase of free energy of 0.16 eV. It is found that the steps related with Li atoms are still downhill in the energy profiles except pathway III that when the first Li^+ adsorbs onto the surface to prepare the reaction, the energy is increased to 0.03 eV. Likewise, in all pathways of Li_2CO_3 nucleations, the intermediary steps together with the

formation of a carbonate still attain the maximum increase of the Gibbs free energy under the equilibrium potential, as well as the energy barriers are found to be the same with the pathways of Li_2CO_3 nucleations at $U = 0$ V. Therefore, the steps involving to the formation of a carbonate in all pathways are the rate-determining steps of Li_2CO_3 nucleation at both the equilibrium potential ($U = U_0(\text{Li}_2\text{CO}_3)$) and open circuit potential ($U = 0$).

When applying the equilibrium potential ($U = U_0(\text{Li}_2\text{C}_2\text{O}_4) = 3.01$ V) of $\text{Li}_2\text{C}_2\text{O}_4$ nucleations on the Au (111) surface, Fig. S8 shows that the Gibbs free energetic profiles of different pathways. The first adsorption of CO_2 molecule on the Au (111) surface as the first step during $\text{Li}_2\text{C}_2\text{O}_4$ nucleations still remain endothermic with the increase of free energy about 0.16 eV, which are the same case with Li_2CO_3 nucleations at equilibrium potential. It is found that in all pathways, the steps related with Li atoms are still all downhill in the energy profiles. The increased free energy to form $\text{C}_2\text{O}_4^{2-}$ is also higher than the intermediary step related with the first adsorption of CO_2 molecules (0.16 eV). Therefore, it is demonstrated that at the equilibrium potential ($U = U_0(\text{Li}_2\text{C}_2\text{O}_4) = 3.01$ V), the step to form $\text{C}_2\text{O}_4^{2-}$ is still the rate-determining step during the $\text{Li}_2\text{C}_2\text{O}_4$ nucleation processes.

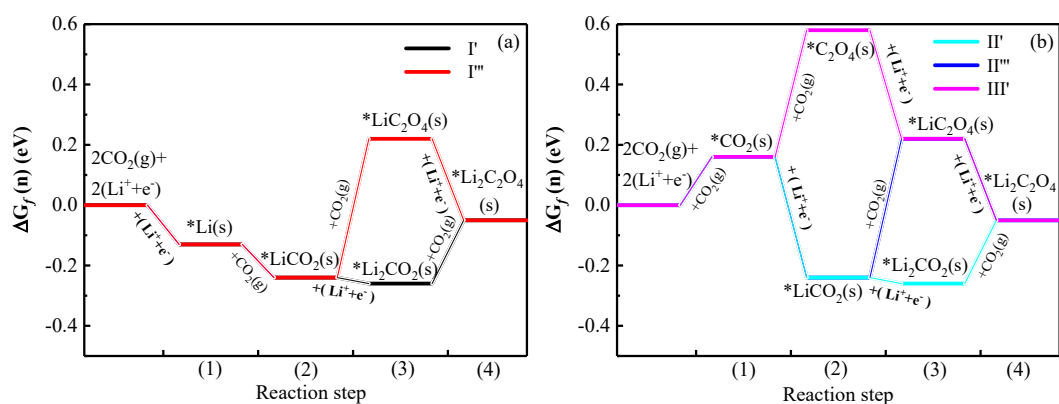


Fig. S8 Calculated energetic profiles of $\text{Li}_2\text{C}_2\text{O}_4$ nucleations on the Au (111) surface at $U = U_0(\text{Li}_2\text{C}_2\text{O}_4) = 3.01$ V.

Table S6 Detailed reaction pathways and corresponding ΔE_{tot} (eV), ΔE_{zpe} (eV), $T\Delta S$ (eV) for the nucleations of Li_2CO_3 or $\text{Li}_2\text{C}_2\text{O}_4$ on Ru (0001) surface

	Reaction step	ΔE_{tot} (eV)	ΔE_{zpe} (eV)	$T\Delta S$ (eV)
I	$\text{Ru} + \text{Li}^+ + \text{e}^- \rightarrow * \text{Li}$	-3.15	0.035	0.10
	$* \text{Li} + \text{CO}_2 \rightarrow * \text{LiCO}_2$	-1.25	0.005	-0.55
	$* \text{LiCO}_2 + \text{Li}^+ + \text{e}^- \rightarrow * \text{Li}_2\text{CO}_2$	-4.14	0.037	0.17
	$* \text{Li}_2\text{CO}_2 + \text{CO}_2 \rightarrow * \text{Li}_2\text{CO}_3 + * \text{CO}$	-0.18	0.030	-0.53
I'	$\text{Ru} + \text{Li}^+ + \text{e}^- \rightarrow * \text{Li}$	-3.15	0.035	0.10
	$* \text{Li} + \text{CO}_2 \rightarrow * \text{LiCO}_2$	-1.25	0.005	-0.55
	$* \text{LiCO}_2 + \text{Li}^+ + \text{e}^- \rightarrow * \text{Li}_2\text{CO}_2$	-3.84	0.047	0.11

	$*Li_2CO_2 + CO_2 \rightarrow *Li_2C_2O_4$	0.17	0.064	-0.44
	$Ru + Li + e \rightarrow *Li$	-3.15	0.035	0.10
I''	$*Li + CO_2 \rightarrow *LiCO_2$	-1.25	0.005	-0.55
	$*LiCO_2 + CO_2 \rightarrow *LiCO_3 + *CO$	0.59	-0.034	-0.49
	$*LiCO_3 + *CO + Li^+ + e^- \rightarrow *Li_2CO_3 + *CO$	-4.92	0.100	0.13
	$Ru + Li^+ + e^- \rightarrow *Li$	-3.15	0.035	0.10
I'''	$*Li + CO_2 \rightarrow *LiCO_2$	-1.25	0.005	-0.55
	$*LiCO_2 + CO_2 \rightarrow *LiC_2O_4$	-0.08	0.034	-0.50
	$*LiC_2O_4 + Li^+ + e^- \rightarrow *Li_2C_2O_4$	-3.59	0.077	0.17
<hr/>				
II	$Ru + CO_2 \rightarrow *CO_2$	-0.52	0.005	-0.41
	$*CO_2 + Li^+ + e^- \rightarrow *LiCO_2$	-3.88	0.035	-0.05
	$*LiCO_2 + CO_2 \rightarrow *LiCO_3 + *CO$	0.59	-0.034	-0.49
	$*LiCO_3 + *CO + Li^+ + e^- \rightarrow *Li_2CO_3 + *CO$	-4.92	0.100	0.13
II'	$Ru + CO_2 \rightarrow *CO_2$	-0.52	0.005	-0.41
	$*CO_2 + Li^+ + e^- \rightarrow *LiCO_2$	-3.88	0.035	-0.05
	$*LiCO_2 + Li^+ + e^- \rightarrow *Li_2CO_2$	-3.84	0.047	0.11
	$*Li_2CO_2 + CO_2 \rightarrow *Li_2C_2O_4$	0.17	0.064	-0.44
II''	$Ru + CO_2 \rightarrow *CO_2$	-0.52	0.005	-0.41
	$*CO_2 + Li^+ + e^- \rightarrow *LiCO_2$	-3.88	0.035	-0.05
	$*LiCO_2 + Li^+ + e^- \rightarrow *Li_2CO_2$	-4.14	0.037	0.17
	$*Li_2CO_2 + CO_2 \rightarrow *Li_2CO_3 + *CO$	-0.18	0.030	-0.53
II'''	$Ru + CO_2 \rightarrow *CO_2$	-0.52	0.005	-0.41
	$*CO_2 + Li^+ + e^- \rightarrow *LiCO_2$	-3.88	0.035	-0.05
	$*LiCO_2 + CO_2 \rightarrow *LiC_2O_4$	-0.08	0.034	-0.50
	$*LiC_2O_4 + Li^+ + e^- \rightarrow *Li_2C_2O_4$	-3.59	0.077	0.17
<hr/>				
III	$Ru + CO_2 \rightarrow *CO_2$	-0.52	0.005	-0.41
	$*CO_2 + CO_2 \rightarrow *CO_3 + *CO$	0.10	-0.001	-0.57
	$*CO_3 + *CO + Li^+ + e^- \rightarrow *LiCO_3 + *CO$	-3.38	0.003	0.04
	$*LiCO_3 + *CO + Li^+ + e^- \rightarrow *Li_2CO_3 + *CO$	-4.92	0.100	0.13
III'	$Ru + CO_2 \rightarrow *CO_2$	-0.52	0.005	-0.41
	$*CO_2 + CO_2 \rightarrow *C_2O_4$	-0.28	0.002	-0.45
	$*C_2O_4 + Li^+ + e^- \rightarrow *LiC_2O_4$	-3.68	0.067	-0.10
	$*LiC_2O_4 + Li^+ + e^- \rightarrow *Li_2C_2O_4$	-3.59	0.077	0.17

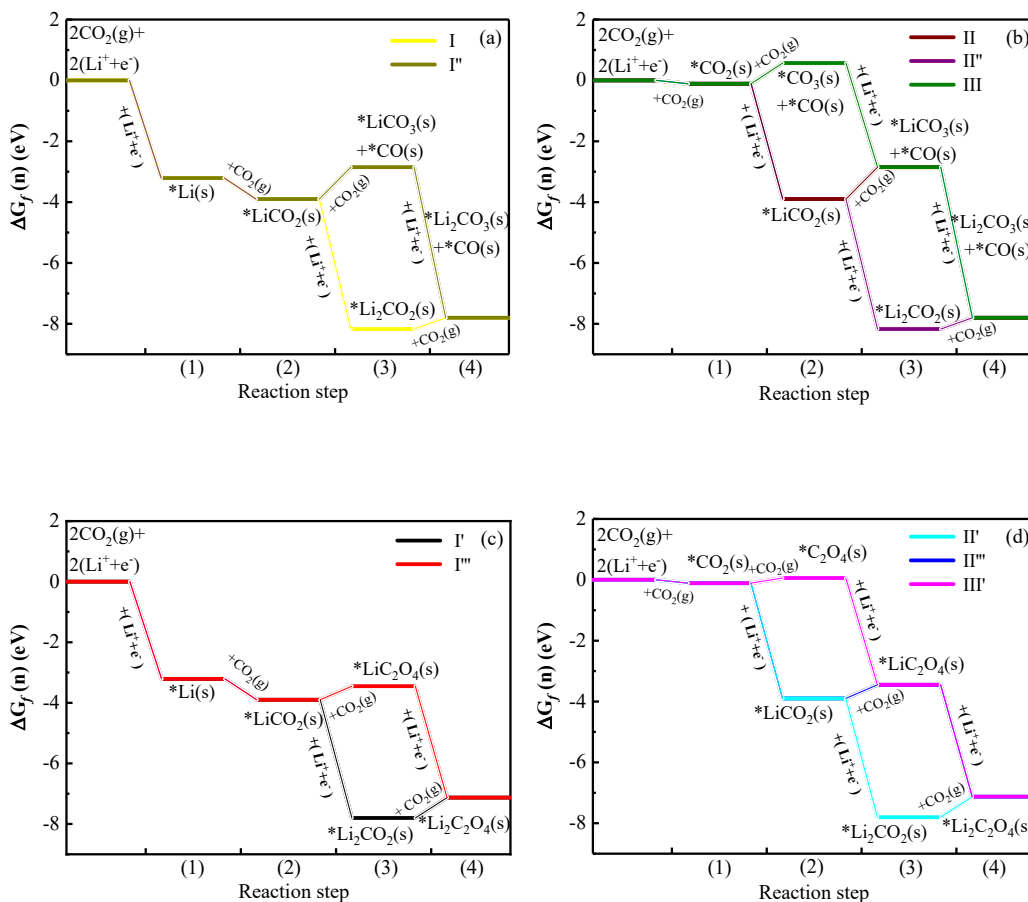


Fig. S9 Calculated energetic profiles of Li_2CO_3 ((a) - (b)) and $\text{Li}_2\text{C}_2\text{O}_4$ ((c) - (d)) on the Ru (0001) surface at $U = 0$ V.

Fig. S9 shows the calculated free energy profiles for Li_2CO_3 and $\text{Li}_2\text{C}_2\text{O}_4$ nucleations on the Ru (0001) surface at an open circuit potential ($U = 0$ V). At first, let us discuss the Li_2CO_3 nucleations processes on the Ru (0001) surface. It is still found that the steps involving the formation of carbonate are the kinetically controlling steps at $U = 0$ V. Likewise, the free energy changes of the controlling steps during all pathways of Li_2CO_3 nucleations on the Ru (0001) surface are observed to 0.37 eV for pathway I, 1.05 eV for pathway I'', 0.37 eV for pathway II'', 1.05 eV for pathway II and 0.67 eV for pathway III, which are slightly less than the energy barriers during Li_2CO_3 nucleations on the Au (111) surface. Next, for the $\text{Li}_2\text{C}_2\text{O}_4$ nucleations, all steps during $\text{Li}_2\text{C}_2\text{O}_4$ nucleations on the Ru (0001) surface are downhill in the Gibbs free energy profiles except the formation of $\text{C}_2\text{O}_4^{2-}$ steps, see Fig. S9 (c)-(d). The free energy changes of the controlling steps during all pathways of $\text{Li}_2\text{C}_2\text{O}_4$ nucleations on the Ru (0001) surface are observed to 0.67 eV for pathway I', 0.45 eV for pathway I''', 0.67 eV for pathway II', 0.45 eV for pathway II''' and 0.17 eV for pathway III'. Likewise, the maximum energetic gaps between two neighbor intermediates during the two pathways (I' and

II') on the Ru (0001) surface (both are 0.67 eV) are found to be larger than those on the Au (111) surface (0.21 eV), while those energetic gaps of the controlling steps during the pathways of I''', II''' and III' on Ru (0001) surfaces are less than those on the Au (111) surface. Therefore, the kinetic rates of the formation of $\text{Li}_2\text{C}_2\text{O}_4$ on the Ru (0001) surface is demonstrated to be possible faster than those on the Au (111) surface during these pathways (I''', II''' and III'). In addition, we find that the first adsorption step of CO_2 molecule on the catalytic Au (111) surface appears the increase of free energy, whereas exhibits the downhill of the free energy on the catalytic Ru (0001) surface, irrespective of Li_2CO_3 nucleations or $\text{Li}_2\text{C}_2\text{O}_4$ nucleations, see Fig. S6 and S9. In addition, the free energy change for the $\text{Li}_2\text{C}_2\text{O}_4$ nucleations on the Ru (0001) surface (-7.14 eV) is also found to be evidently less than that on the Au (111) surface (-6.07 eV), indicating the $\text{Li}_2\text{C}_2\text{O}_4$ nucleations thermodynamically much more favorable on the Ru (0001) catalytic surface than on Au (111) surface. Likewise, during Li_2CO_3 nucleations, the Gibbs free energy change on the Ru (0001) surface (-7.8 eV) is also far less than that on Au (111) surface (-6.22 eV). In particular, the Gibbs free energy changes during Li_2CO_3 nucleation on the catalytic Ru (0001) and Au (111) surfaces are all less than those during $\text{Li}_2\text{C}_2\text{O}_4$ nucleations.

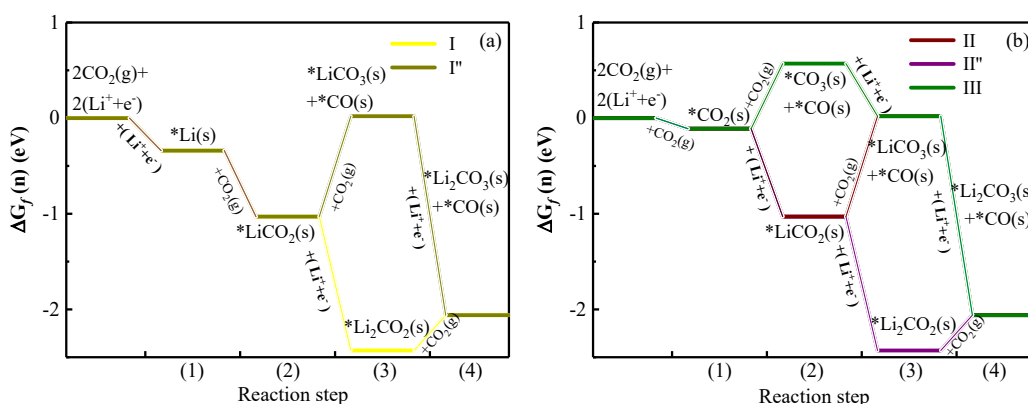


Fig. S10 Calculated energetic profiles of Li_2CO_3 nucleations on the Ru (0001) surface at $U = U_0(\text{Li}_2\text{CO}_3) = 2.87$ V.

Fig. S10 shows the Gibbs free energetic profiles of Li_2CO_3 nucleations on the Ru (0001) surface under the equilibrium potential ($U = U_0(\text{Li}_2\text{CO}_3) = 2.87$ V). When applying the equilibrium potential, the intermediary steps along with the formation a carbonate are still the kinetically controlling steps during the Li_2CO_3 nucleations on the Ru (0001) surface. The energy changes of the controlling steps during all pathways on the Ru (0001) surface are found to be slightly lower than those on the Au (111) surface irrespective of the equilibrium potential and open circuit potential. In addition, the total Gibbs free energy changes for Li_2CO_3 nucleations on the Ru (0001) surface are also found to be slightly lower than that on the Au (111) surface,

indicating the Li_2CO_3 nucleations thermodynamically much more favorable on the Ru (0001) catalytic surface. Therefore, the catalytic surface of Ru (0001) thermodynamically exhibits better catalytic performance for Li_2CO_3 nucleations.

Fig. S11 shows the Gibbs free energetic profiles of $\text{Li}_2\text{C}_2\text{O}_4$ nucleations on the Ru (0001) surface under the equilibrium potential ($U = U_0(\text{Li}_2\text{C}_2\text{O}_4) = 3.01 \text{ V}$). All steps during $\text{Li}_2\text{C}_2\text{O}_4$ nucleations on the Ru (0001) surface are still downhill in the Gibbs free energy profiles except the formation of $\text{C}_2\text{O}_4^{2-}$ steps, compared with the Gibbs free energetic profiles at $U = 0 \text{ V}$, see Fig. S9 (c) and (d). Compared with the $\text{Li}_2\text{C}_2\text{O}_4$ nucleations on the Au (111) surface, it is found that the change trends in all the pathways on the Ru (0001) surface (see Fig. S11) are similar to those on the Au (111) surface (see Fig. S8) surface except that the adsorption of CO_2 in the first intermediary step are keeping downhill in the free energy profiles on Ru (0001) surfaces (see Fig. S11 (b)).

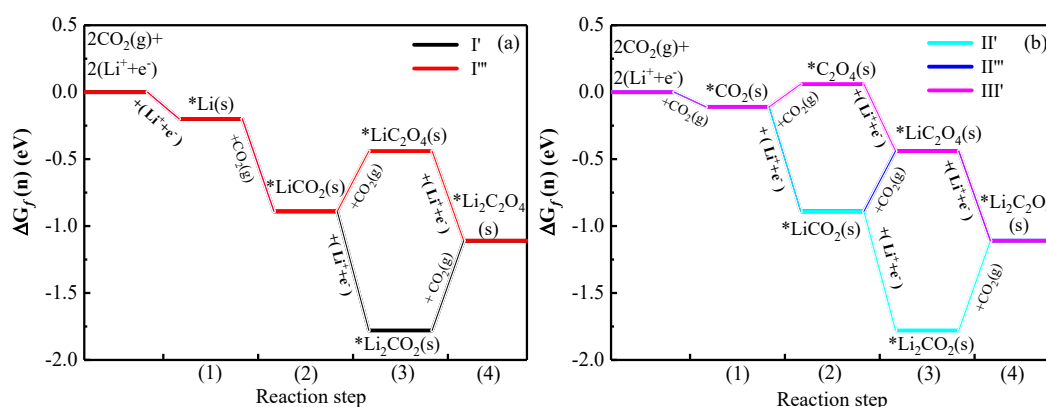


Fig. S11 Calculated energetic profiles of $\text{Li}_2\text{C}_2\text{O}_4$ on the Ru (0001) surface at $U = U_0(\text{Li}_2\text{C}_2\text{O}_4) = 3.01 \text{ V}$.

From thermodynamically standpoints, the total Gibbs free energy changes during Li_2CO_3 nucleations on the catalytic Ru (0001) and Au (111) surfaces are all less than those during $\text{Li}_2\text{C}_2\text{O}_4$ nucleations, as well as the total Gibbs free energy changes for Ru surface are all less than those on Au surface irrespective of Li_2CO_3 or $\text{Li}_2\text{C}_2\text{O}_4$ nucleations. In other regards of kinetically views, the energetic gaps of the controlling steps for Ru (0001) surfaces are found less than those Au (111) surfaces, indicating the kinetic rates on the Ru (0001) surface would be possible faster than those on the Au (111) surfaces for Li_2CO_3 nucleations. For $\text{Li}_2\text{C}_2\text{O}_4$ nucleations, the kinetic rates on the Ru (0001) surface is demonstrated to be possible faster than those on the Au (111) surface during these pathways (I'', II'' and III'), but during the other two pathways, the kinetic rates on the Ru (0001) surface would be slower than those on Au (111) surface. Therefore, the catalytic surface of Ru (0001) thermodynamically and kinetically exhibits better catalytic performance for

Li₂CO₃ nucleations.

Table S7 The rate-determining step and calculated discharge overpotential η_0 for the Li₂CO₃ (red) and Li₂C₂O₄ (black) nucleations on Au and Ru catalytic surfaces at the equilibrium potential

catalytic surface		I	I'	I''	I'''	II	II'	II''	II'''	III	III'
Au (111)	η_0/eV	0.49	0.21	1.35	0.46	1.35	0.21	0.49	0.46	0.79	0.42
Ru (0001)	η_0/eV	0.37	0.67	1.05	0.45	1.05	0.67	0.37	0.45	0.67	0.17

The overpotential (η_0) for the Li₂CO₃ and Li₂C₂O₄ nucleations on the precious Au and Ru catalytic surfaces can be obtained on the basis of the Gibbs free energy change of the controlling step $\Delta G_f(n)$, which is defined in Eq. (4). A lower η_0 indicate less energy barriers to overcome, that is to say, this step is easily to realize.

$$\eta_0 = -\frac{\Delta G_f(n)}{e} \quad (4)$$

It is well known that the best possible pathways are determined at the equilibrium potentials during Li-CO₂ batteries or electrocatalysis, but at open circuit potential during the common thermal catalysis. The calculated overpotential (η_0) for the Li₂CO₃ and Li₂C₂O₄ nucleations on the Au and Ru catalytic surfaces at the equilibrium potential can be found in Table S7. During the Li₂CO₃ nucleations, the controlling steps on Au and Ru catalytic surfaces are the intermediary steps involving the formation of a carbonate. According to the calculated overpotential (η_0) listed in Table S7, the minimum overpotentials (η_0) are 0.49 V on Au (111) surfaces and 0.37 V on Ru (0001) surfaces during the pathways of both I and II''. However, for Au (111) surface, the overpotential in the next controlling step of pathway I ($\eta_0 = -0.11$ V) is less than the pathway II'' ($\eta_0 = 0.16$ V), while for Ru (0001) surface, the overpotential in the next controlling step of pathway I ($\eta_0 = -0.34$ V) is also less than the pathway II'' ($\eta_0 = -0.11$ V). Therefore, pathway I during the Li₂CO₃ nucleations is demonstrated to be the favorable pathway on both Au (111) and Ru (0001) surfaces.

During the process of Li₂C₂O₄ nucleations on the Au (111) and Ru (0001) surface, the controlling steps on Au and Ru catalytic surfaces are the intermediary steps involving the formation of an oxalate. The calculated minimum overpotentials (η_0) are 0.21 V on the Au (111) surface for the pathways (I' and II') and 0.17 V on the Ru (0001) surface for the pathway III', respectively. However, for the Au (111) surface, the overpotential in the next controlling step of the pathway I' ($\eta_0 = -0.02$ V) is less than the pathway II'' ($\eta_0 = 0.16$ V). Therefore, the Li₂C₂O₄ nucleations on the Au (111) and Ru (0001) surfaces possibly follow the pathways I' and III', respectively.

In addition, by checking all pathways at open circuit potentials, the best possible pathways are still the pathway I' on Au surface and III' on Ru surface for $\text{Li}_2\text{C}_2\text{O}_4$ nucleations, and the pathway I on both Au and Ru surface for Li_2CO_3 nucleations.

S6. Gibbs free energy change during the decomposition process of Li_2CO_3

Table S8 Detailed reaction pathways and corresponding ΔE_{tot} (eV), ΔE_{zpe} (eV), $T\Delta S$ (eV) for the decompositions of Li_2CO_3 on Au (111) and Ru (0001) surfaces

	Reaction step	ΔE_{tot} (eV)	ΔE_{zpe} (eV)	$T\Delta S$ (eV)
Path _{D1} (Au)	$\text{Li}_2\text{CO}_3(\text{s}) + \text{Au} \rightarrow 2\text{Li}^+ + 2\text{e}^- + * \text{CO}_3$	7.09	0.132	-0.090
	$* \text{CO}_3 \rightarrow * \text{CO}_2 + * \text{O}$	-0.13	0.020	-0.005
	$* \text{CO}_2 + * \text{O} \rightarrow \text{CO}_2 (\text{g}) + * \text{O}$	0.25	-0.008	0.403
	$* \text{O} + \text{Li}_2\text{CO}_3(\text{s}) \rightarrow * \text{O} + 2\text{Li}^+ + 2\text{e}^- + * \text{CO}_3$	7.09	0.132	-0.090
	$* \text{O} + * \text{CO}_3 \rightarrow * \text{O} + * \text{CO}_2 + * \text{O}$	-0.13	0.020	-0.005
	$* \text{O} + * \text{CO}_2 + * \text{O} \rightarrow * \text{O} + \text{CO}_2 (\text{g}) + * \text{O}$	0.25	-0.008	0.403
	$* \text{O} + * \text{O} \rightarrow * \text{O}_2$	0.61	0.015	-0.005
	$* \text{O}_2 \rightarrow \text{O}_2 (\text{g})$	1.01	0.016	0.505
Path _{D2} (Au)	$\text{Li}_2\text{CO}_3(\text{s}) + \text{Au} \rightarrow 2\text{Li}^+ + 2\text{e}^- + * \text{CO}_3$	7.09	0.132	-0.090
	$* \text{CO}_3 \rightarrow * \text{CO}_2 + * \text{O}$	-0.13	0.020	-0.005
	$* \text{CO}_2 + * \text{O} \rightarrow \text{CO}_2 (\text{g}) + * \text{O}$	0.25	-0.008	0.403
	$\text{C}(\text{s}) + * \text{O} \rightarrow * \text{CO}$	0.76	0.129	0.100
	$* \text{CO} + \text{Li}_2\text{CO}_3(\text{s}) \rightarrow * \text{CO} + 2\text{Li}^+ + 2\text{e}^- + * \text{CO}_3$	7.09	0.132	-0.090
	$* \text{CO} + * \text{CO}_3 \rightarrow * \text{CO} + * \text{CO}_2 + * \text{O}$	-0.13	0.020	-0.005
	$* \text{CO} + * \text{CO}_2 + * \text{O} \rightarrow * \text{CO} + \text{CO}_2 (\text{g}) + * \text{O}$	0.25	-0.008	0.403
	$* \text{CO} + * \text{O} \rightarrow * \text{CO}_2$	-0.67	0.057	0.069
$* \text{CO}_2 \rightarrow \text{CO}_2 (\text{g})$	0.25	-0.008	0.403	
Path _{D1} (Ru)	$\text{Li}_2\text{CO}_3(\text{s}) + \text{Ru} \rightarrow 2\text{Li}^+ + 2\text{e}^- + * \text{CO}_3$	5.92	0.158	-0.105
	$* \text{CO}_3 \rightarrow * \text{CO}_2 + * \text{O}$	-0.23	-0.046	0.007
	$* \text{CO}_2 + * \text{O} \rightarrow \text{CO}_2 (\text{g}) + * \text{O}$	0.52	-0.005	0.405
	$* \text{O} + \text{Li}_2\text{CO}_3(\text{s}) \rightarrow * \text{O} + 2\text{Li}^+ + 2\text{e}^- + * \text{CO}_3$	5.92	0.158	-0.105
	$* \text{O} + * \text{CO}_3 \rightarrow * \text{O} + * \text{CO}_2 + * \text{O}$	-0.23	-0.046	0.007
	$* \text{O} + * \text{CO}_2 + * \text{O} \rightarrow * \text{O} + \text{CO}_2 (\text{g}) + * \text{O}$	0.52	-0.005	0.405
	$* \text{O} + * \text{O} \rightarrow * \text{O}_2$	4.68	-0.006	0.060
	$* \text{O}_2 \rightarrow \text{O}_2 (\text{g})$	2.34	0.017	0.486
Path _{D2} (Ru)	$\text{Li}_2\text{CO}_3(\text{s}) + \text{Ru} \rightarrow 2\text{Li}^+ + 2\text{e}^- + * \text{CO}_3$	5.92	0.158	-0.105
	$* \text{CO}_3 \rightarrow * \text{CO}_2 + * \text{O}$	-0.23	-0.046	0.007
	$* \text{CO}_2 + * \text{O} \rightarrow \text{CO}_2 (\text{g}) + * \text{O}$	0.52	-0.005	0.405
	$\text{C}(\text{s}) + * \text{O} \rightarrow * \text{CO}$	0.15	0.097	0.096
	$* \text{CO} + \text{Li}_2\text{CO}_3(\text{s}) \rightarrow * \text{CO} + 2\text{Li}^+ + 2\text{e}^- + * \text{CO}_3$	5.92	0.158	-0.105
	$* \text{CO} + * \text{CO}_3 \rightarrow * \text{CO} + * \text{CO}_2 + * \text{O}$	-0.23	-0.046	0.007
	$* \text{CO} + * \text{CO}_2 + * \text{O} \rightarrow * \text{CO} + \text{CO}_2 (\text{g}) + * \text{O}$	0.52	-0.005	0.405
	$* \text{CO} + * \text{O} \rightarrow * \text{CO}_2$	-0.49	0.062	0.079
$* \text{CO}_2 \rightarrow \text{CO}_2 (\text{g})$	0.52	-0.005	0.405	

S7. Electrochemical Free energy during the discharge and charge processes

The electrochemical free energy change (ΔG_E (M)) of the intermediates on different catalytic surfaces are calculated as:¹⁰

$$\Delta G_E(M) = E_{\text{tol}} - E_{\text{su}} + N_{\text{Li}}(\mu_{\text{Li}} - eU) + N_{\text{CO}_2}\mu_{\text{CO}_2} + N_{\text{C}}\mu_{\text{C}} \quad (5)$$

where E_{tol} and E_{su} are the total energy of the intermediates on the Au (111) and Ru (0001) surfaces and the energy of the metal surfaces. N_{Li} , N_{C} and N_{CO_2} are the number of Li, C and CO_2 adsorbed on the surface. μ_{Li} , μ_{C} and μ_{CO_2} are the chemical potentials of Li, C atom and CO_2 molecules, which are obtained from a single Li or C atom in bulk and a single CO_2 molecule in the gas phase, respectively. U is the electromotive force dependent of the external potential in an electrochemical reaction, which can easily change the chemical potential of an electron.¹¹⁻¹⁴ To confirm the electrochemical performance on the Au (111) and Ru (0001) surfaces, the charge (U_{C}) and discharge (U_{DC}) electrode potentials are obtained as the minimum and maximum electrode potentials, causing that all steps in the best pathway remain energetically downhill. $U_{\text{eq,DC}}$ and $U_{\text{eq,C}}$ are equivalent to the thermodynamic equilibrium potential to driving the discharge and charge processes to occur spontaneously. The calculated overpotentials for discharging (η_{DC}) and charging (η_{C}) are calculated as:

$$\eta_{\text{DC}} = U_{\text{eq,DC}} - U_{\text{DC}} \quad (6)$$

$$\eta_{\text{C}} = U_{\text{C}} - U_{\text{eq,C}} \quad (7)$$

and $\eta_{\text{TOT}} = \eta_{\text{C}} + \eta_{\text{DC}}$.

References

- 1 X. J. Liu, L. Sun and W. Q. Deng, *J. Phys. Chem. C*, 2018, **122**, 8306-8314.
- 2 X. Feng, J. I. Cerda and M. Salmeron, *J. Phys. Chem. Lett.*, 2015, **6**, 1780-1784.
- 3 Y. Qiao, J. Yi, S. C. Wu, Y. Liu, S. X. Yang, P. He and H. S. Zhou, *Joule*, 2017, **1**, 359-370.
- 4 C. Yang, K. Guo, D. Yuan, J. Cheng and B. Wang, *J. Am. Chem. Soc.*, 2020, **142**, 6983-6990.
- 5 Z. Zhang, W. L. Bai, Z. P. Cai, J. H. Cheng, H. Y. Kuang, B. X. Dong, Y. B. Wang, K. X. Wang and J. S. Chen, *Angew. Chem. Int. Ed. Engl.*, 2021, **60**, 16404-16408.
- 6 J. F. Xie, Q. Liu, Y. Y. Huang, M. X. Wu and Y. B. Wang, *J. Mater. Chem. A*, 2018, **6**, 13952-13958.
- 7 J. Zhou, X. Li, C. Yang, Y. Li, K. Guo, J. Cheng, D. Yuan, C. Song, J. Lu and B. Wang, *Adv. Mater.*, 2019, **31**, e1804439.
- 8 V. Wang, N. Xu, J.-C. Liu, G. Tang and W.-T. Geng, *Comput. Phys. Commun.*, 2021, **267**, 108033.
- 9 Y. Jing and Z. Zhou, *ACS Catal.*, 2015, **5**, 4309-4317.
- 10 Y. Mo, S. P. Ong and G. Ceder, *Phys. Rev. B*, 2011, **84**, 205446.

- 11 C. Chowdhury and A. Datta, *PCCP*, 2018, **20**, 16485-16492.
- 12 J. S. Hummelshøj, A. C. Luntz and J. K. Nørskov, *J. Chem. Phys.*, 2013, **138**, 034703.
- 13 J. S. Hummelshøj, J. Blomqvist, S. Datta, T. Vegge, J. Rossmeisl, K. S. Thygesen, A. C. Luntz, K. W. Jacobsen and J. K. Nørskov, *J. Chem. Phys.*, 2010, **132**, 071101.
- 14 R. Choi, J. Jung, G. Kim, K. Song, Y.-I. Kim, S. C. Jung, Y.-K. Han, H. Song and Y.-M. Kang, *Energy Environ. Sci.*, 2014, **7**, 1362-1368.